Increasing Fisher Information using Moving-Mesh Reconstruction

Qiaoyin Pan,[1,2,*] Ue-Li Pen,[2,3,4,5,†] Derek Inman,[2,6] and Hao-Ran Yu[2,7]

[1]*School of Physics, Nankai University, 94 Weijin Rd, Nankai, Tianjin, 300071, China*
[2]*Canadian Institute for Theoretical Astrophysics, University of Toronto, 60 St. George Street, Toronto, Ontario M5S 3H8, Canada*
[3]*Dunlap Institute for Astronomy and Astrophysics, University of Toronto, Toronto, ON M5S 3H4, Canada*
[4]*Canadian Institute for Advanced Research, Program in Cosmology and Gravitation*
[5]*Perimeter Institute for Theoretical Physics, Waterloo, ON, N2L 2Y5, Canada*
[6]*Department of Physics, University of Toronto, 60 St. George, Toronto, ON M5S 1A7, Canada*
[7]*Kavli Institute for Astronomy and Astrophysics, Peking University, Beijing 100871, China*

(Dated: December 6, 2016)

Reconstruction techniques are commonly used in cosmology to reduce complicated nonlinear behaviour to a more tractable linearized system. We study the Moving-Mesh algorithm which is able to consistently compute the displacement field from non-linear density fields. To quantify the algorithm's ability to reconstruct linear modes, we study the Fisher information presented in 136 N-body simulations before and after reconstruction. We find that the linear scale is pushed to $k \simeq 0.3$ h/Mpc after reconstruction. We furthermore find that the translinear plateau of the cumulative Fisher information is increased by a factor of ~ 40 after reconstruction, from $I \simeq 2.5 \times 10^{-5}/(\mathrm{Mpc/h})^3$ to $I \simeq 10^{-3}/(\mathrm{Mpc/h})^3$ at $k \simeq 1$ h/Mpc. This result includes the decorrelation between initial and final fields, which has been neglected in some previous studies artificially improving their performance. We expect this technique to be beneficial to problems such as baryonic acoustic oscillations and cosmic neutrinos that rely on an accurate disentangling of nonlinear evolution from underlying linear effects.

PACS numbers:

I. INTRODUCTION

Two-point statistics provide a complete description of Gaussian density fields and can be computed efficiently even for large data sets. However, non-linear gravitational evolution leads to highly non-Gaussian matter distributions which require higher order statistics to fully characterize. Such statistics are computationally expensive and can be challenging to relate to cosmological parameters. To mitigate these difficulties, it is common to transform the matter field in a way that hopefully reduces non-Gaussianity. For example, Gaussianization transforms have been used to make the logarithmic distribution more Gaussian [1, 2] and Wavelet Non-Linear Wiener filters have been used to separate Gaussian and non-Gaussian components of the density field [3–5].

The success of techniques can be quantified by computing the Fisher information present in the power spectrum before and after reconstruction. For linear fields, the Fisher information is simply proportional to the number of modes (k^3). Rimes and Hamilton [6] were the first to study the Fisher information in the non-linear matter power spectrum calculated from N-body simulations. They found that the information has a plateau on translinear scales ($k \simeq 0.2 - 0.8\ h$/Mpc) due to strong coupling of Fourier modes. Qualitatively, this means that the power spectrum on small scales gives little additional information. However, Harnois-Déraps et al. [5] computed the Fisher information for various Gaussianization methods (and combinations of methods) and found that while mode coupling is reduced, there is not necessarily an improvement in the cross correlation between the initial Gaussian density field and the final non-linear one.

In studies of Baryon Acoustic Oscillations (BAO), density fields are subjected to *reconstruction* which partially inverts non-linear evolution by applying a negative displacement field. This field is typically computed via Lagrangian perturbation theory (LPT) using the linear Zel'Dovich displacement, $-\nabla_q \cdot \boldsymbol{\Psi}(\boldsymbol{q})$ with respect to initial coordiantes $\boldsymbol{q}$ [7]. Recently, Zhu et al. [8] described how to use the Moving Mesh algorithm (MM), first described in [9, 10], to consistently compute $\boldsymbol{\Psi}(\boldsymbol{q})$ even for non-linear density fields. They further showed that even though shell-crossing and vorticity are not recovered, information is still recovered on scales relevent tot he BAO.

In this paper, we compute the Fisher information recovered after using this reconstruction scheme on 136 independent N-body simulations. The paper is organized as follows. In §II and III, we briefly describe the computation of the displacement potential using MM reconstruction and the N-body simulations used for the Fisher information computation. In §IV, we compute the power spectra, correlation matrix and Fisher information before and after reconstruction. Finally, in §V, we discuss the effectiveness of the reconstruction and its potential uses.

II. RECONSTRUCTION ALGORITHM

In this section, we briefly review the MM algorithm; for a more complete description we refer the reader to

*Electronic address: panda@mail.nankai.edu.cn
†Electronic address: pen@cita.utoronto.ca

[8]. The general principle is to relate a particles Eulerian coordinates, x^i to a curvilinear system, ξ^μ, in which the number of particles per grid cell is approximately constant. These coordinates are related via the so-called deformation, which we assume to be a pure gradient:

$$x^i = \xi^\mu \delta^i_\mu + \frac{\partial \phi}{\partial \xi^\mu} \delta^{i\mu} \tag{1}$$

and ϕ is called the deformation potential. We can solve for the potential via the continuity equation:

$$\partial_\mu (\rho \sqrt{g} e^\mu_i \delta^{i\nu} \partial_\nu \dot{\phi}) = \Delta\rho. \tag{2}$$

where $e^i_\mu = \partial x^i / \partial \xi^\mu$ is the coordinate transformation matrix, $\sqrt{g} \equiv \det |e^i_\mu|$ is the volume element and $\Delta\rho = \bar{\rho} - \rho\sqrt{g}$. We note that the assumption of constant mass per volume allowed us to set $\partial(\sqrt{g}\rho)/\partial t = 0$ in the computation. Eq. 2 can be solved through the use of the multigrid algorithm described in [9–11]. The displacement field is then given by...

III. N-BODY SIMULATIONS AND POWER SPECTRA

We use the CUBEP^{3}M code [12] to run 136 simulations with a box size of 300 Mpc/h and 512^3 particles. The initial conditions are computed using the transfer function given by CAMB [13] and then propagating the power back to $z = 100$ with a linear growth factor. The Zel'dovich approximation is used to calculate the displacement and velocity fields of the particles. For these simulations, we use cosmological parameters $\Omega_M = 0.321$, $\Omega_\Lambda = 1.0 - \Omega_m$, $h = 0.67$, $\sigma_8 = 0.83$, and $n_s = 0.96$. Different random seeds are used to produce the initial conditions for different simulations so that they are independent of each other.

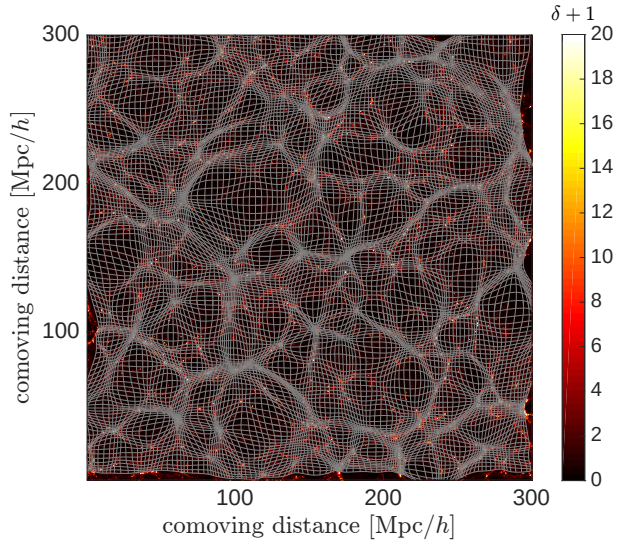

FIG. 1: The 2-D projection of the deformed grid of a sample N-body simulations is shown as curved white lines. The density fluctuation, $\delta\rho/\bar{\rho}$, is shown underneath.

We use Cloud-In-Cell (CIC) interpolation to estimate the density contrast $\delta_S = \delta\rho/\rho - 1$ from the particles. We then apply the MM reconstruction to these fields with a resolution of 128^3 cells. A 2D projection of the deformed grids and the original density field are given in Fig. 1. As expected, there is no grid crossing after reconstruction.

The cross power spectrum, $P_{ij}(k)$, is defined as

$$\langle \delta_i(\boldsymbol{k}) \delta_j(\boldsymbol{k'}) \rangle = (2\pi)^3 P_{ij}(k) \delta_D(\boldsymbol{k} - \boldsymbol{k'}), \tag{3}$$

where δ_i and δ_j are density contrasts and δ_D is the Dirac delta funciton. We typically consider instead the dimensionless power spectrum, $\Delta^2_{ij}(k)$, defined as

$$\Delta^2_{ij}(k) \equiv \frac{k^3 P_{ij}(k)}{2\pi^2}. \tag{4}$$

In the left panel of Fig. 2, we show the matter auto power spectrum ($i = j$) of linear theory density fields (δ_L), from the simulation results (δ_S) and after reconstruction ($\delta_R = -\nabla^2\phi$). For the simulation and reconstruction results, we use the average value of all 136 simulations and show 1σ variances as error bars. To determine the correlation between fields, we compute the cross correlation coefficient $r_{ij}(k) = P_{ij}/\sqrt{P_{ii}P_{jj}}$. In the right panel of Fig. 2, we show r_{SL} and r_{RL}. We see that the reconstructed field is much more highly correlated with the linear field than the simulation field is. Specifically, we find that the scale at which $r(k) = 1/2$ drops from $k \simeq 0.2$ h/Mpc to 0.6 h/Mpc. In comparison with the results of Zhu et al. [11], we find the correlation coefficient falls off at slightly lower wavenumbers which we attribute to using lower resolution simulations.

IV. FISHER INFORMATION CONTENT

Mathamatically, the Fisher information I of the initial scale invariant matter power spectrum, A, is defined as

$$I_A \equiv -\left\langle \frac{\partial^2 \ln\mathcal{L}}{\partial A^2} \right\rangle, \tag{5}$$

in which $\mathcal{L}$ denotes the likelihood [14]. For Gaussian fluctuations, the likelihood depends on parameters only through the power spectrum $P(k)$, so I can be written as

$$I_A = -\left\langle \sum_{k,k'} \frac{\partial \ln P(k)}{\partial \ln A} \frac{\partial^2 \ln\mathcal{L}}{\partial \ln P(k) \partial \ln P(k')} \frac{\partial \ln P(k')}{\partial \ln A} \right\rangle, \tag{6}$$

in which the angle bracket denotes the average of many realizations of the power spectrum [6].

Eq. 6 can be written in a simpler form in two aspects. First, we can simplify the derivative terms $\partial P/\partial A$. For any density field δ_i, we can conveniently decompose it into linear and non-linear components

$$\delta_(k) = b(k)\delta_L(k) + \delta_N(k), \tag{7}$$

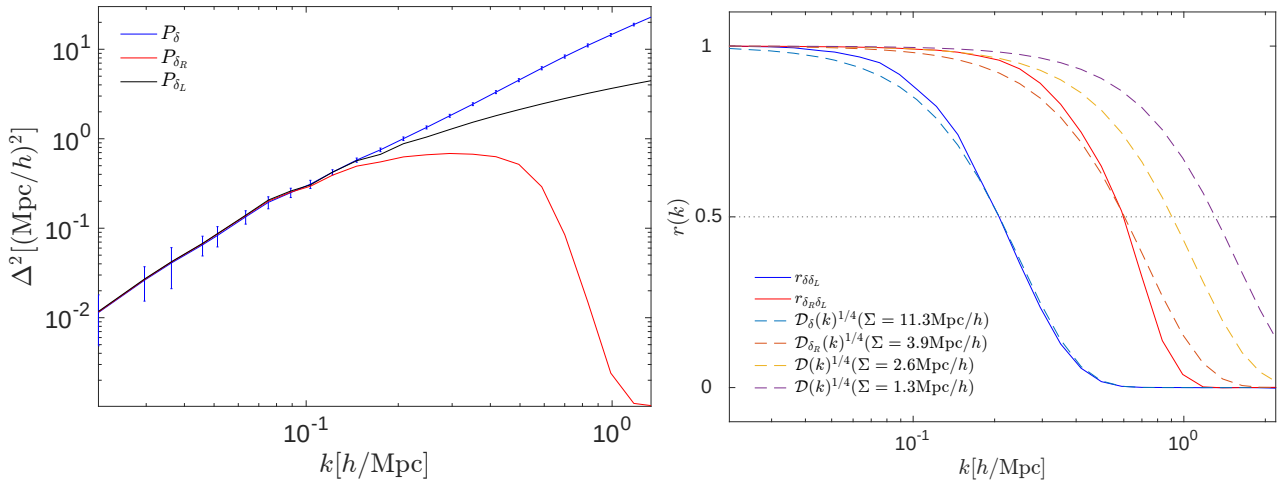

FIG. 2: *Left.* The dimensionless power spectrum computed via linear theory (black), the mean value of 136 N-body simulations with 1σ error bars (blue), and reconstruction of the simulations (red). *Right.* The cross correlation function (solid lines) r_{SL} (blue) and r_{RL} (red), and BAO damping models (dash lines).

in which δ_L denotes the linear density field, $b(k)$ is the bias and $\delta_N(k)$ is defined such that the correlation $\langle\delta_L(k)\delta_N(k)\rangle$ is zero. If we correlate δ_i and δ_L,

$$\langle\delta_i(k)\delta_L(k)\rangle = b(k)\langle\delta_L(k)\delta_L(k)\rangle, \tag{8}$$

we can solve for b as

$$b(k) = \frac{P_{iL}(k)}{P_{LL}(k)}. \tag{9}$$

To find the non-linear term, we correlate δ_i with itself,

$$\langle\delta_i(k)\delta_i(k)\rangle = b^2(k)\langle\delta_L(k)\delta_L(k)\rangle + \langle\delta_N(k)\delta_N(k)\rangle, \tag{10}$$

and find

$$P_{ii}^2(k) = b^2(k)P_{LL}(k) + P_{NN}(k). \tag{11}$$

With the help of Eq. 9 and Eq. 11, we can replace the partial derivatives $\partial\ln P(k)/\partial\ln A$ in Eq. 6 with r_{iL}^2.

The second step we can make is to simplify $\partial^2\ln\mathcal{L}/\partial\ln P(k)\partial\ln P(k')$ by utilizing the fact that its expectation value is the Fisher matrix. For linear fields, this is equal to the inverse of the covariance matrix which is diagonal with elements given by the number of modes in each bin. We can extend this definition to non-linear fields, provided we take into account that the covariance matrix is no longer diagonal and invert it appropriately. Thus, we can write the Fisher information in terms of matrix multiplication:

$$I_A\,(<k_n) = r^2(k)^{\mathrm{T}}\left[\mathrm{C}_{\mathrm{norm}}^{-1}(k,k')\right]_{<k_n} r^2(k'), \tag{12}$$

where $\mathrm{C}_{\mathrm{norm}}$ is the normalized covariance matrix defined as

$$\mathrm{C}_{\mathrm{norm}}\,(k,k') = \frac{\mathrm{Cov}(k,k')}{\langle P(k)\rangle\langle P(k')\rangle}, \tag{13}$$

r is the mean cross correlation of a given density field with linear one and the subscript $< k_n$ indicates the matrix is set to zero for modes $k, k' > k_n$. The covariance matrix is defined as

$$\mathrm{Cov}\,(k,k') \equiv \frac{\sum_{i,j=1}^{N}\left[P_i\,(k) - \langle P\,(k)\rangle\right]\left[P_j\,(k') - \langle P\,(k')\rangle\right]}{N-1}, \tag{14}$$

where N is the total number of simulations and angle brackets are values averaged over all simulations.

The correlation matrix is the normalized version of the covariance matrix:

$$\mathrm{Corr}\,(k,k') = \frac{\mathrm{Cov}\,(k,k')}{\sqrt{\mathrm{Cov}\,(k,k)\,\mathrm{Cov}\,(k',k')}}, \tag{15}$$

and represents the correlation between different k modes. The corelation matrices for non-linear and reconstructed power spectra are shown in the upper and lower sections of Fig. 3. By definition, the correlation matrix is symmetrix with unit diagonal allowing us to overlay the two matrices. For the non-linear case, the correlation matrix is almost diagonal linear regime $k \lesssim 0.07$ h/Mpc. The off-diagonal elements are produced by strong mode coupling on non-linear scales and the super-survey tidal effect which is small on linear scales but dominates in the weakly non-linear regime [15]. The correlation matrix for the nonlinear power spectra has few negative elements ($\mathrm{Corr} \gtrsim -0.1$), which should vanish with more simulations [16]. For the reconstructed correlation matrix, the linear regime expands up to $k \simeq 0.3$ h/Mpc. However, the number and magnitude of negative off-diagonal elements also increases ($\mathrm{Corr} \gtrsim -0.8$).

We plot the cumulative Fisher information per volume of the nonlinear, linear and reconstructed power spectra in Fig. 4(a). The Fisher information of the non-linear power spectra drops from the linear one at $k \simeq 0.05$ h/Mpc, and has a flat plateau in the translinear regime, $k \simeq 0.3$ h/Mpc, with a saturated value of $I \simeq 2.5 \times 10^{-5}/(\mathrm{Mpc/h})^3$. This indicates that there

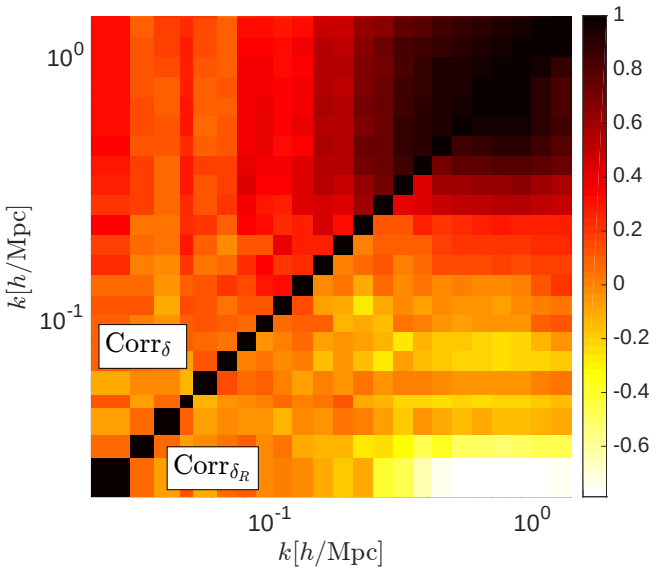

FIG. 3: The correlation matrix as found from 136 non-linear power spectra (the upper-left elements) and the reconstructed power spectra (the lower-right off-diagonal elements).

is nearly no independent information in the translinear regime. However, the information curve of the reconstructed power spectra keeps increasing roughly the same as the linear information until $k \simeq 0.3$ h/Mpc, and reaches its plateau at $k \simeq 0.8$ h/Mpc with a value of $I \simeq 10^{-3}/(\mathrm{Mpc/h})^3$, up by a factor of 40. It means that the MM reconstructed method can strongly recover the lost information within these scales. We compare the Fisher information given by the MM reconstruction method with the logarithmic density mapping method [2] as an example to illustrate its strength. We find that the MM reconstruction gives 10 times more information than the logarithmic mapping. In some papers, the cross correlation r^2 terms are set to unity in Eq. 12, which artificially increases the information. For comparison, we plot this case in Fig. 4(b). We see that the logarithmic density mapping information is much higher, but only because it is not well correlated with the initial conditions.

V. CONCLUSION

The MM reconstruction method successfully recovers the lost linear information on mildly non-linear scales and increases the saturated information from $I \simeq 2.5 \times 10^{-5}/((\mathrm{Mpc/h})^3)$ to at least $I \simeq 10^{-3}/(\mathrm{Mpc/h})^3$. The result is better than previous methods, e.g. [2–4, 17], and we may improve further as the correlation coefficient between the reconstructed and linear fields will increase with higher resolution simulations [11]. This successful result on cold dark matter density fields provides strong motivation to adapt the MM reconstruction scheme to other cosmological fields such as biased tracers like halos and other matter components like baryons and neutrinos.

Acknowledgments

We thank Hong-Ming Zhu,Yu Yu and Xin Wang for friendly and helpful discussions. Computations were performed on the General Purpose Cluster supercomputer at the SciNet HPC Consortium. SciNet is funded by: the Canadian Foundation for Innovation under the auspices of Compute Canada; the Government of Ontario; Ontario Research Fund - Research Excellence; and the University of Toronto.

[1] D. H. Weinberg, MNRAS **254**, 315 (1992).
[2] M. C. Neyrinck, I. Szapudi, and A. S. Szalay, ApJ **698**, L90 (2009), 0903.4693.
[3] T.-J. Zhang, H.-R. Yu, J. Harnois-Déraps, I. MacDonald, and U.-L. Pen, ApJ **728**, 35 (2011), 1008.3506.
[4] H.-R. Yu, J. Harnois-Déraps, T.-J. Zhang, and U.-L. Pen, MNRAS **421**, 832 (2012), 1012.0444.
[5] J. Harnois-Déraps, H.-R. Yu, T.-J. Zhang, and U.-L. Pen, MNRAS **436**, 759 (2013), 1205.4989.
[6] C. D. Rimes and A. J. S. Hamilton, MNRAS **360**, L82 (2005), astro-ph/0502081.
[7] Y. B. Zel'dovich, A&A **5**, 84 (1970).
[8] H.-M. Zhu, U.-L. Pen, and X. Chen, ArXiv e-prints (2016), 1609.07041.
[9] U.-L. Pen, ApJS **100**, 269 (1995).
[10] U.-L. Pen, ApJS **115**, 19 (1998), astro-ph/9704258.
[11] H.-M. Zhu, Y. Yu, U.-L. Pen, X. Chen, and H.-R. Yu (2016), 1611.09638.
[12] J. Harnois-Déraps, U.-L. Pen, I. T. Iliev, H. Merz, J. D. Emberson, and V. Desjacques, MNRAS **436**, 540 (2013), 1208.5098.
[13] A. Lewis, A. Challinor, and A. Lasenby, ApJ **538**, 473 (2000), astro-ph/9911177.
[14] M. Tegmark, A. N. Taylor, and A. F. Heavens, ApJ **480**, 22 (1997), astro-ph/9603021.
[15] K. Akitsu, M. Takada, and Y. Li, ArXiv e-prints (2016), 1611.04723.
[16] R. Takahashi, N. Yoshida, M. Takada, T. Matsubara, N. Sugiyama, I. Kayo, A. J. Nishizawa, T. Nishimichi, S. Saito, and A. Taruya, ApJ **700**, 479 (2009), 0902.0371.
[17] M. C. Neyrinck, I. Szapudi, and C. D. Rimes, MNRAS **370**, L66 (2006), astro-ph/0604282.

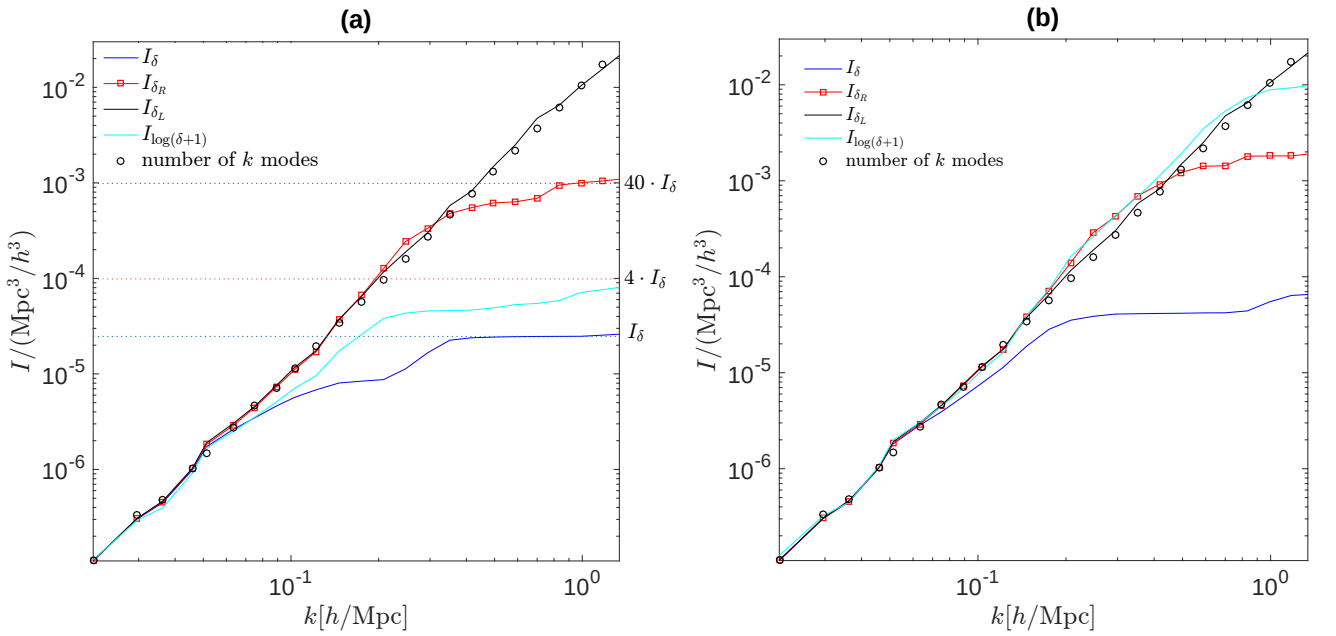

FIG. 4: (a) The cumulative Fisher information per unit volume as a function of wavenumber. The blue line corresponds to the non-linear density fields, the red line with squares corresponds to the the reconstructed density fields, the dark line corresponds to the linear density fields, the cyan line corresponds to the logarithmic density mapping, and the circles are $\propto k^3$. Dotted lines correspond 4 and 40 times the saturated value of the non-linear Fisher information. (b) Same as (a) except with $r \equiv 1$. The black, blue and cyan lines match the results in [2, 6].